

Complex magnetic structure in $\text{Ba}_5\text{Ru}_3\text{O}_{12}$ with isolated Ru_3O_{12} trimer

T. Basu^{1,*}, F. Y. Wei,² Q. Zhang³, Y. Fang² and X. Ke¹

¹*Department of Physics and Astronomy, Michigan State University, East Lansing, Michigan 48824, USA*

²*Jiangsu Laboratory of Advanced Functional Materials, Department of Physics, Changshu Institute of Technology, Changshu 215500, China*

³*Neutron Scattering Division, Oak Ridge National Laboratory, Oak Ridge, Tennessee 37831, USA*



(Received 7 July 2020; accepted 6 October 2020; published 2 November 2020)

We report detailed magnetic, transport, heat-capacity, and neutron-diffraction measurements of $\text{Ba}_5\text{Ru}_3\text{O}_{12}$, a compound consisting of isolated Ru_3O_{12} trimers. We show that this system develops long-range antiferromagnetic ordering at $T_N \sim 60$ K without structural distortion or metal-insulator type transition, which is in sharp contrast to other barium ruthenate trimer systems such as 9R-BaRuO_3 and $\text{Ba}_4\text{Ru}_3\text{O}_{10}$. A complex magnetic structure is revealed which is attributable to the magnetic frustration due to competing exchange interactions between Ru ions on different crystallographic sites within the Ru_3O_{12} trimer and different degree of orbital hybridization on different Ru sites. We have also investigated the magnetic structure of $\text{Ba}_4\text{Ru}_3\text{O}_{10}$ for comparisons.

DOI: [10.1103/PhysRevMaterials.4.114401](https://doi.org/10.1103/PhysRevMaterials.4.114401)

I. INTRODUCTION

The interplay between electronic correlation of extended $4d$ orbital, crystal-field effect, and strong spin-orbit coupling in ruthenates yields a rich variety of physical properties, such as superconductivity, Mott insulator, orbital ordering, quantum spin liquid, metal-insulator transition, multiferroicity, etc. [1–8]. Because of the ground-state instability due to such competing effects, a small external perturbation, e.g., doping, pressure, magnetic field, can readily modify the electronic and magnetic correlations and thus the ground-state properties of systems even in the same family [3,9–11]. For example, among the ARuO_3 ($A = \text{Ca}, \text{Sr}, \text{Ba}$) ruthenate family, SrRuO_3 with orthorhombic perovskite structure is an itinerant ferromagnet below 165 K [12], whereas the isostructural compound CaRuO_3 is a paramagnetic non-Fermi liquid metal [13]. On the other hand, the isochemical compound BaRuO_3 , where the Ba cation has larger ionic radius compared to Sr/Ca, crystallizes in hexagonal or rhombohedral perovskite structure [four(4H)-, six(6H), or nine(9R)-layered structures] that depends on the synthesis condition, and thus exhibits various physical properties [14].

In particular, 9R-BaRuO_3 (space group $R-3m$), which consists of corner-sharing Ru_3O_{12} trimers, shows a metal-insulator type (semiconductor-insulator) transition around 110 K which is accompanied by a structural change, a feature distinct from hexagonal BaRuO_3 [15]. No long-range magnetic ordering is observed for all BaRuO_3 compounds (Ru^{+4} , $S = 1$ in low-spin state) [15]. In contrast, $\text{Ba}_4\text{Ru}_3\text{O}_{10}$, which crystallizes in orthorhombic structure (space group $Cmca$) and consists of chains of Ru_3O_{10} trimers running along the c axis in a zigzag manner [16–19], exhibits a metal-insulator type (semiconductor-insulator) transition around 105

K that is accompanied by antiferromagnetic (AFM) ordering but no structural transition. In addition, $\text{Ba}_4Ln\text{Ru}_3\text{O}_{12}$ ($Ln = \text{La}$, rare earth), which has an average valence state of $+4.33/\text{Ru}$ (when $Ln = Ln^{+3}$), is isostructural to 9R-BaRuO_3 (space group $R-3m$) and consists of similar Ru_3O_{12} trimers, though the trimers connected through $Ln\text{O}_6$ octahedra. Nevertheless, different from 9R-BaRuO_3 , $\text{Ba}_4Ln\text{Ru}_3\text{O}_{12}$ does not exhibit any structural or metal-insulator type transition and undergoes long-range magnetic ordering at low temperature. The long-range ordering in semiconducting $\text{Ba}_4Ln\text{Ru}_3\text{O}_{12}$ with Ln being magnetic rare-earth atom is understood to be triggered by the rare-earth magnetic ordering. Intriguingly, $\text{Ba}_4\text{LaRu}_3\text{O}_{12}$, where Ru_3O_{12} trimers are connected via non-magnetic La atom, also exhibits long-range magnetic ordering at ~ 6 K, which is in sharp contrast to 9R-BaRuO_3 . Similarly, isostructural compound $\text{Ba}_4\text{NbRu}_3\text{O}_{12}$ with a different valence state of Ru ($+3.67/\text{Ru}$ for Ru_3O_{12} trimers) behaves as a Mott insulator and magnetically orders around 4 K with a strong geometrical frustration. Therefore, both valence state and local crystal environment of Ru ion play an important role on the physical properties of ruthenates even in the similar family. The small structural change/distortion can significantly modify magnetic correlation and spin-lattice coupling, which leads to vastly different ground states and intriguing physical properties.

The title compound, $\text{Ba}_5\text{Ru}_3\text{O}_{12}$ (an average valence state of $+4.67/\text{Ru}$), which has nearly similar crystal structure to the aforementioned 9R-BaRuO_3 , $\text{Ba}_4\text{Ru}_3\text{O}_{10}$, or $\text{Ba}_4Ln(\text{Nb})\text{Ru}_3\text{O}_{12}$, crystallizes in $Pnma$ space group and consists of Ru_3O_{12} trimers (Fig. 1). Each trimer is composed of face-sharing RuO_6 octahedra, similar to other ruthenates mentioned above. Nevertheless, in contrast to other barium ruthenates, the Ru_3O_{12} trimers of $\text{Ba}_5\text{Ru}_3\text{O}_{12}$ are not connected to each other [16]. Interestingly, despite the isolated trimer structure, a previous report of magnetic susceptibility suggests that $\text{Ba}_5\text{Ru}_3\text{O}_{12}$ exhibits an AFM ordering below

*tathamaybasu@gmail.com

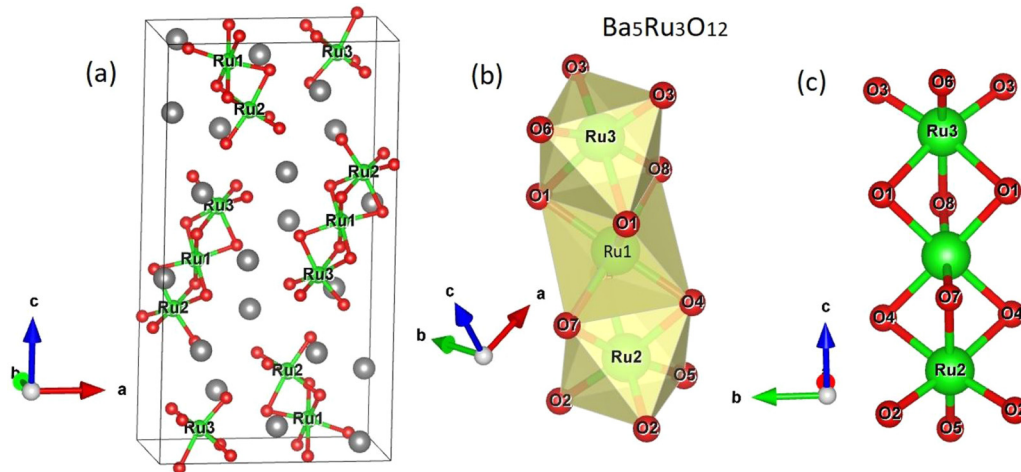


FIG. 1. Crystal structure of $\text{Ba}_5\text{Ru}_3\text{O}_{12}$. The Ru trimers are shown in (b), (c).

60 K [16]. Despite that there are some studies of trimer ruthenates where trimers are connected, thus far only a brief report exists on this isolated trimer system [16]. Therefore, it is highly desirable to investigate $\text{Ba}_5\text{Ru}_3\text{O}_{12}$ in detail to study the nature of its magnetic ground state and to better understand the electronic and magnetic correlation in this trimer system.

In this paper we have reported comprehensive magnetic, transport, heat-capacity, and neutron-diffraction measurements on $\text{Ba}_5\text{Ru}_3\text{O}_{12}$. We have revealed a complex antiferromagnetic spin structure below $T_N \sim 60$ K which is presumably ascribed to combining effects of competing magnetic exchange interactions between Ru ions on different crystallographic sites and different orbital hybridization on different Ru sites. Neither structural phase transition nor a change in electronic properties is observed to accompany the onset of magnetic ordering. A brief comparison to the magnetic structure of $\text{Ba}_4\text{Ru}_3\text{O}_{10}$ is also presented.

II. EXPERIMENTAL DETAILS

The polycrystalline $\text{Ba}_5\text{Ru}_3\text{O}_{12}$ sample was synthesized using solid-state chemistry method by mixing high-quality (>99.9%) chemical of BaCO_3 and RuO_2 , as described in earlier report [16]. The stoichiometric mixture of raw materials was pressed into pellets and sintered in air at 600°C for 24 h and then taken out to regrind. After repeating three cycles of this process, the powder was pressed into pellets and then sintered at 1200°C for 24 h. Magnetic susceptibility measurements as a function of temperature and magnetic field were performed using a commercial superconducting quantum interference device–vibrating-sample magnetometer. The resistivity and heat-capacity measurements were conducted using Physical Properties Measurements System. Neutron powder diffraction measurements were carried out using a high-resolution time-of-flight neutron powder diffractometer (POWGEN) with a bandwidth with central wavelengths of 2.665 \AA in Oak Ridge National Laboratory. A POWGEN automatic changer was used to cover the temperature region of 10–300 K. The magnetic structure was resolved using FULLPROF package and SARAH program [20,21].

III. RESULTS

A. Magnetic properties

The DC magnetic susceptibility ($\chi = M/H$) as a function of temperature in the presence of 1-kOe magnetic field is shown in Fig. 2(a). The paramagnetic Curie-Weiss (C-W) behavior deviates below 120 K, implying the development of short-range correlation. With further lowering the temperature χ starts to decrease sharply below ~ 60 K (T_N), manifesting a well-defined long-range AFM ordering. The C-W fit [$\chi = \chi_0 + c/(T - \Theta_{CW})$] between 200–350 K yields Curie temperature (Θ_{CW}) of -118 K and an effective magnetic moment (μ_{eff}) of $4.42 \mu_B$ per formula unit, with negligible $\chi_0 = -0.00013$ emu/mol. The negative value of Θ_{CW} indicates dominant AFM interactions in this system. The Θ_{CW} is higher than T_N , suggesting magnetic frustration with a frustration parameter ($|\Theta_{CW}/T_N|$) ~ 2 . The isothermal magnetization [$M(H)$] below T_N [as shown in Fig. 2(b) for $T = 3$ and 40 K] exhibits a linear behavior as a function of magnetic field, supporting the AFM nature of this compound.

B. Heat capacity and resistivity

The temperature-dependent heat capacity (C) measured at $H = 0$ and 50 kOe is plotted in Fig. 2(c). The peak below T_N confirms the magnetic ordering of this compound. We do not observe any appreciable change at $H = 50$ kOe, suggesting that the associated Zeeman energy is much smaller than the dominant magnetic exchange interaction. It is likely that there is already entropy loss at higher temperature as a result of short-range magnetic correlation from trimer. Thus, the change in entropy loss is low around the magnetic ordering temperature, which yields a small peak in the heat capacity. We have also measured DC resistivity for the titled compound. The resistivity increases exponentially with lowering the temperature down to 10 K [see inset of Fig. 2(a)], which indicates insulating behavior (with an activation energy of 0.05 eV) of this compound. An insulating behavior is also reported in $\text{Ba}_4\text{Ln}(\text{Nb})\text{Ru}_3\text{O}_{12}$ [4]. No metal-insulator transition is observed, unlike BaRuO_3 or $\text{Ba}_4\text{Ru}_3\text{O}_{10}$ [15,18].

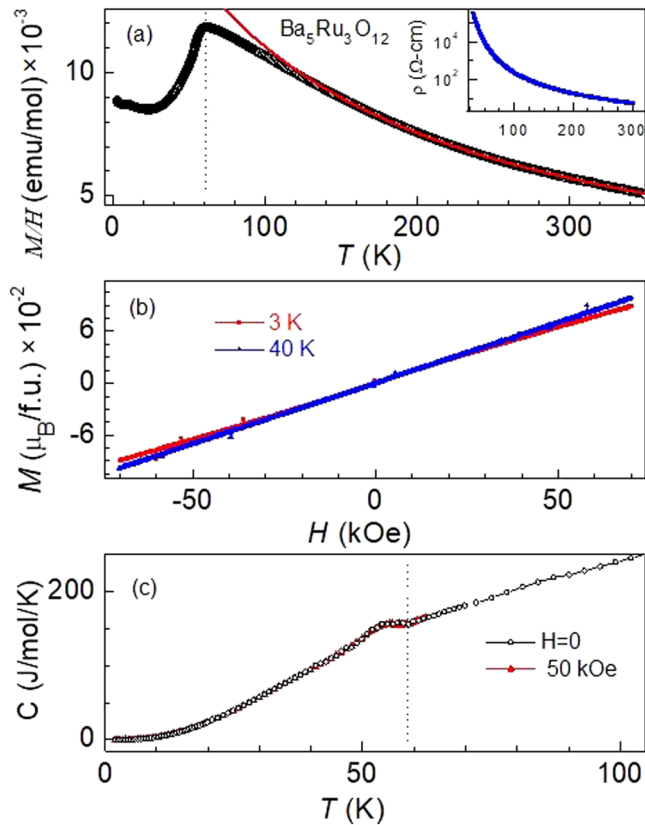


FIG. 2. (a) The temperature-dependent DC magnetic susceptibility measured with 1-kOe magnetic field. The red curve is the Curie-Weiss fit in paramagnetic region from 200 to 350 K. The inset shows the resistivity as a function of temperature measured at zero magnetic field. (b) Isothermal magnetization as a function of magnetic field at $T = 3$ and 40 K. (c) Heat capacity as a function of temperature measured at $H = 0$ and 50 kOe.

C. Neutron powder diffraction

We have performed neutron powder diffraction measurements to resolve the magnetic structure of $\text{Ba}_5\text{Ru}_3\text{O}_{12}$. The neutron-diffraction profile measured at 100 K (above T_N) is well fitted with the reported space group $Pnma$, as shown in Fig. 3(a), which affirms single phase of the material. For $\text{Ba}_5\text{Ru}_3\text{O}_{12}$ there are three distinct inequivalent Ru sites in Ru_3O_{12} trimer [i.e., Ru1, Ru2, Ru3 (Fig. 1)] but with same Wyckoff position $4c$ ($x, 1/4, z$). This is distinct from other trimer systems discussed above which have only two inequivalent Ru sites with different Wyckoff positions. The atomic position of Ru1 (the middle Ru atom of the trimer), Ru2, and Ru3 in $\text{Ba}_5\text{Ru}_3\text{O}_{12}$ are (0.7859, 0.25, 0.5575), (0.8806, 0.25, 0.6735), and (0.6935, 0.25, 0.4309), respectively (Fig. 1). It is worth noting that the bond length between Ru1 and Ru2 is ~ 2.51 Å, whereas it is ~ 2.69 Å between Ru1 and Ru3. RuO_6 octahedra are slightly distorted and the distortion is different for different Ru sites. The bond angles of O-Ru-O are tabulated in Table I.

The neutron-diffraction pattern as a function of the momentum transfer (Q) measured at $T = 10$ and 100 K is plotted in Fig. 3(b), which shows the change of Bragg peak intensity below and above T_N . At $T = 10$ K, besides the enhanced

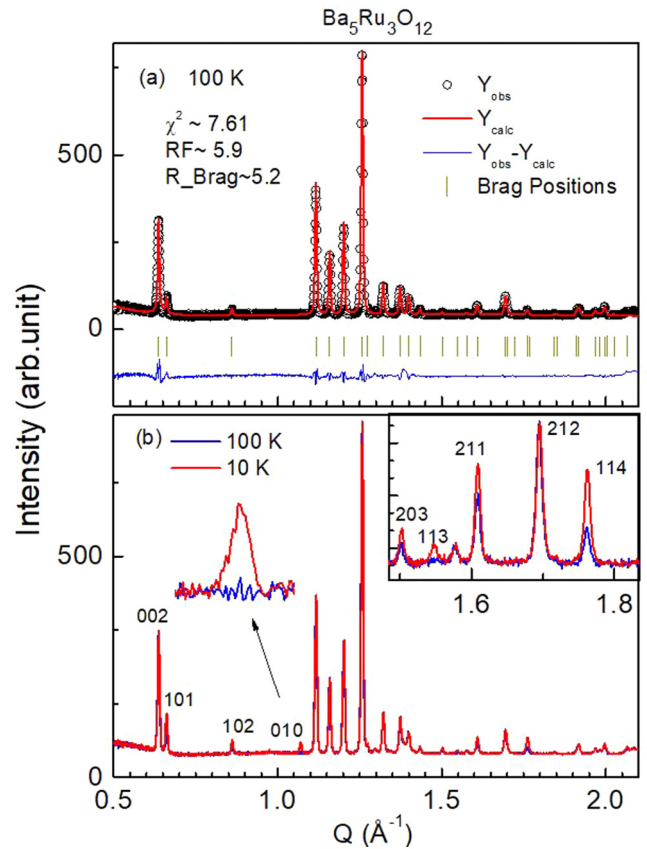


FIG. 3. (a) Rietveld refinement to the neutron powder diffraction pattern measured at $T = 100$ K. The open black circle represents the experimental data, while the red solid line shows the Rietveld fitting. The vertical bars display the Bragg peak positions of crystal structure. The continuous blue line at the bottom shows the difference between the experimental and calculated intensity. (b) Comparison of neutron powder diffraction pattern collected at $T = 10$ and 100 K. The inset shows an expanded view at higher Q . The $(H K L)$ values are indexed for most of reflections.

intensity of some of Bragg reflections compared to the 100 K data, an additional Bragg peak is observed at $Q \sim 1.07$ Å⁻¹ that corresponds to (0 1 0). Furthermore, no structural change is observed at 10 K compared to that of 100 K, which excludes any structural phase transition accompanying the magnetic transition.

The propagation vector is found to be $\mathbf{k} = (000)$. The irreducible representations (I.R.) and basis vectors (B.V.) of the Ru1 spins for $Pnma$ space group associated with the propagation vector, obtained from SARAH program, are shown in

TABLE I. The O-Ru-O bond of RuO_6 octahedron angle for different Ru and oxygen sites for $\text{Ba}_5\text{Ru}_3\text{O}_{12}$.

<O-Ru1-O	<O-Ru2-O	<O-Ru3-O
<O8-Ru1-O1 82.9°	<O7-Ru2-O4 84.0°	<O8-Ru3-O1 79.4°
<O1-Ru1-O4 93.7°	<O4-Ru2-O2 92.8°	<O1-Ru3-O3 98.4°
<O4-Ru1-O7 88.7°	<O2-Ru2-O5 94.5°	<O3-Ru3-O6 95.8°
<O7-Ru1-O8 173.4°	<O5-Ru2-O7 172.7°	<O6-Ru3-O8 164.9°
<O1-Ru1-O4 178.3°	<O2-Ru2-O4 173.8°	<O1-Ru3-O3 171.1°

TABLE II. The irreducible representations and basis vectors for each Ru site (4c) for space group $Pnma$ and the propagation vector $\mathbf{k} = (000)$.

I.R.	B.V.	x, y, z			$x + 1/2, -y + 1/2, -z + 1/2$			$-x, y + 1/2, -z$			$-x + 1/2, -y, z + 1/2$		
		m_a	m_b	m_c	m_a	m_b	m_c	m_a	m_b	m_c	m_a	m_b	m_c
Γ_1	Ψ_1	0	2	0	0	-2	0	0	2	0	0	-2	0
Γ_2	Ψ_2	2	0	0	2	0	0	-2	0	0	-2	0	0
	Ψ_3	0	0	2	0	0	-2	0	0	-2	0	0	2
Γ_3	Ψ_4	2	0	0	2	0	0	2	0	0	2	0	0
	Ψ_5	0	0	2	0	0	-2	0	0	2	0	0	-2
Γ_4	Ψ_6	0	2	0	0	-2	0	0	-2	0	0	2	0
Γ_5	Ψ_7	0	2	0	0	2	0	0	2	0	0	2	0
Γ_6	Ψ_8	2	0	0	-2	0	0	-2	0	0	2	0	0
	Ψ_9	0	0	2	0	0	2	0	0	-2	0	0	-2
Γ_7	Ψ_{10}	2	0	0	-2	0	0	2	0	0	-2	0	0
	Ψ_{11}	0	0	2	0	0	2	0	0	2	0	0	2
Γ_8	Ψ_{12}	0	2	0	0	2	0	0	-2	0	0	-2	0

Table II. Because of the same Wyckoff site of three Ru atoms, obviously Ru2 and Ru3 atoms have exactly the same I.R. and B.V. as Ru1 atom. There are eight irreducible representations for each Ru atom, as represented by $\Gamma_{\text{mag}}(\text{Ru}) = 1\Gamma_1^1 + 2\Gamma_2^1 + 2\Gamma_3^1 + 1\Gamma_4^1 + 1\Gamma_5^1 + 2\Gamma_6^1 + 2\Gamma_7^1 + 1\Gamma_8^1$. The magnetic moments along crystallographic a , b , and c axes are described by $\Psi_2(\Gamma_2)$, $\Psi_4(\Gamma_3)$, $\Psi_8(\Gamma_6)$, $\Psi_{10}(\Gamma_7)$ B.V., $\Psi_1(\Gamma_1)$, $\Psi_6(\Gamma_4)$, $\Psi_7(\Gamma_5)$, $\Psi_{12}(\Gamma_8)$ B.V., and $\Psi_3(\Gamma_2)$, $\Psi_5(\Gamma_3)$, $\Psi_9(\Gamma_6)$, $\Psi_{11}(\Gamma_7)$ B.V., respectively. Since neutrons couple to the magnetic moment component perpendicular to \mathbf{Q} , the absence of noticeable difference in the (0 0 2) Bragg peak intensity measured at 10 and 100 K suggests that the magnetic moment is oriented along c , or at least the c component of magnetic moment (M_c) is dominant. First, we consider the basis functions which only have M_c component, that is, $\Psi_3(\Gamma_2)$, $\Psi_5(\Gamma_3)$, $\Psi_9(\Gamma_6)$, and $\Psi_{11}(\Gamma_7)$. Among these basis functions, $\Psi_9(\Gamma_6)$ yields best profile matching in Rietveld refinement, as shown in Fig. 4(a). The obtained magnetic structure is illustrated in Fig. 5(a) where magnetic moments are collinearly aligned along the c axis. Ru1 and Ru2 spins are parallel aligned, while Ru1 and Ru3 spins are antiparallel aligned. This is reasonable considering FM direct exchange interaction between Ru1 and Ru2 due to metallic bond length (less than Ru-Ru bond ~ 2.65 Å in Ru metal) and the antiferromagnetic superexchange interaction of Ru1-O-Ru3 bond. The FM direct exchange interaction between Ru1 and Ru2 is expected to compete with the Ru1-O-Ru2 AFM superexchange interaction, giving rise to magnetic frustration. We notice that although the refinement using $\Psi_9(\Gamma_6)$ basis function nearly captures the extra magnetic Bragg peak (0 1 0) and the enhanced Bragg peak intensity of most of nuclear reflections, there is a mismatch in experimentally and theoretically obtained intensity of the (1 1 4) reflection [see inset of Fig 4(a)]. In addition, the negligible change in the intensity of (2 0 0) Bragg peak between 10 and 100 K suggests the possibility of a component of magnetic moment (M_a). Thus, we have tried a combination of basis functions which can give magnetic moment in ac plane. We find that the low-temperature neutron-scattering data are best fitted using a combination of $\Psi_2(\Gamma_2)$ and $\Psi_9(\Gamma_6)$, as shown in Fig. 4(b). For instance, as shown in the inset of Fig. 4(b), both (0 1 0) and (1 1 4) Bragg

peaks are much better fitted using this model compared to those using the other earlier one [see the inset of Fig. 4(a)]. The obtained magnetic structure based on this refinement is

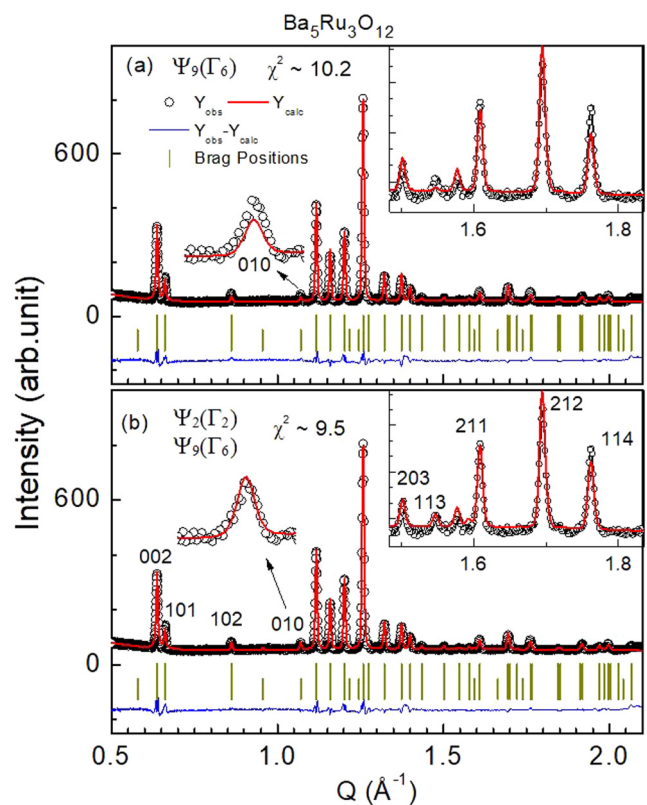


FIG. 4. Rietveld refinement to the neutron powder diffraction pattern measured at $T = 10$ K modeled with (a) $\Psi_9(\Gamma_6)$ only and (b) a combination of $\Psi_2(\Gamma_2)$ and $\Psi_9(\Gamma_6)$. The open black circles represent the experimental data, while the red solid curve shows the Rietveld fitting. The vertical bars display the Bragg peak positions of crystal structure; the next lower vertical lines represent magnetic Bragg peaks associated with the propagation vector $\mathbf{k} = (000)$. The continuous blue line at the bottom of the figure shows the difference between the experimental and calculated intensity. The insets show an expanded view of some Bragg reflections.

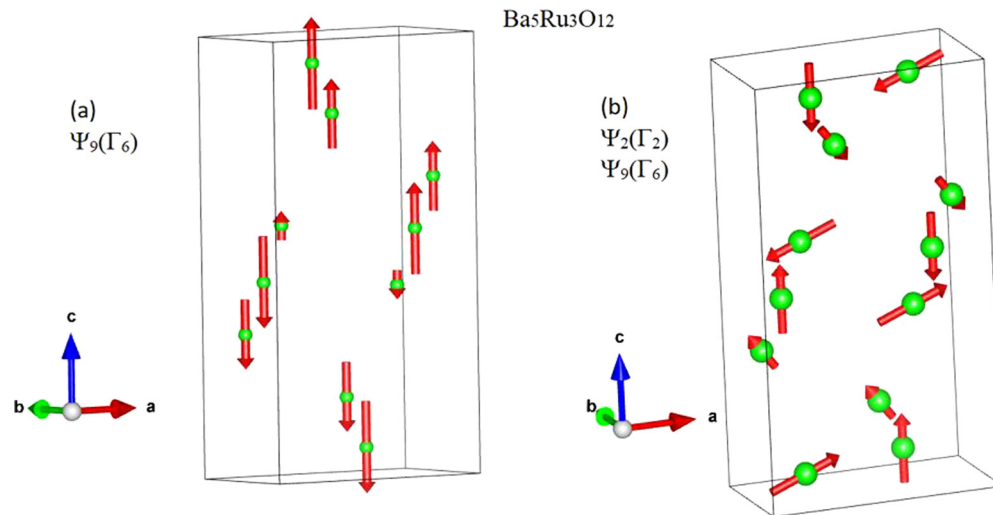


FIG. 5. Magnetic structure of $\text{Ba}_5\text{Ru}_3\text{O}_{12}$ modeled with (a) $\Psi_9(\Gamma_6)$ only and (b) a combination of $\Psi_2(\Gamma_2)$ and $\Psi_9(\Gamma_6)$. The arrow denotes relative moment size of the Ru atoms.

depicted in Fig. 5(b). The magnetic moments are noncollinear and confined in the ac plane. The moment of Ru1 (middle of trimer) is oriented along the c axis, and the moments of Ru2 and Ru3 are oriented in ac plane with a canting angle of 74.4° and 62° relative to the c axis. The moment size of Ru1, Ru2, Ru3 is $\sim 1.52, 1.36,$ and $0.91 \mu_B$, respectively. This yields a total moment of $3.79 \mu_B$ per Ru_3O_{12} trimer.

Such a canted magnetic structure possibly arises from different competing nearest-neighbor and next-nearest-neighbor interactions between different inequivalent Ru sites. Based on Goodenough-Anderson-Kanamori rules, the nearest-neighbor exchange interactions (J_{nn}) includes (i) Ru1-Ru2 ferromagnetic direct exchange interaction, (ii) Ru1-O-Ru2 AFM superexchange interaction, and (iii) Ru1-O-Ru3 AFM superexchange interaction. However, the next-nearest-neighbor super-superexchange interactions (J_{nnn}) between Ru1 and Ru3 in the trimer may not be negligible. The competition among J_{nn} and J_{nnn} , where $J_{nnn} < J_{nn}$, introduces exchange frustration and therefore may stabilize the system with a canted spin structure. The neighboring trimers are antiferromagnetically coupled via the super-superexchange interaction (i.e., Ru1-O-O-Ru1), which yields 3D long-range AFM ordering.

A temperature- and d -dependent neutron-scattering intensity map is shown in Fig. 6. One can see that the $(0\ 1\ 0)$ reflection emerges and the intensity of $(1\ 0\ 2)$ becomes enhanced below 60 K, which further confirms the magnetic ordering.

We have also performed the neutron-scattering measurements on another trimer ruthenate $\text{Ba}_4\text{Ru}_3\text{O}_{10}$ for comparison, which is documented in the Supplemental Material [22]. The good fitting of Rietveld refinement at 140 K (Fig. S2a in the Supplemental Material [22]) confirms the desired structure with $Cmca$ space group as reported earlier [18]. The Rietveld refinement at 10 K is depicted in Fig. S2b in the Supplemental Material [22]. A preliminary neutron-diffraction study by Klein *et al.* [18] documented an enhancement on (002) peak below magnetic ordering and proposed a magnetic structure. In addition to (002) Bragg peak, we have observed an

enhancement of the neutron-diffraction intensity of some other additional Bragg peaks compared to the data taken at 140 K. Some of those magnetic Bragg peaks are depicted in insets of Fig. S2a in the Supplemental Material [22]. All these peaks are well modeled with propagation vector $\mathbf{k} = (0\ 0\ 0)$ (see Fig. S2b and insets in the Supplemental Material [22]). The magnetic structure obtained from the refinement confirms the prediction of earlier report by Klein *et al.* [18]. There is no magnetic moment on Ru1, thereby the trimer essentially behaves like a dimer, which is distinct from $\text{Ba}_5\text{Ru}_3\text{O}_{12}$. The moment on Ru2 is $1.05 \mu_B$ and points to the b direction. The spins on Ru2 are antiferromagnetically coupled within a trimer. The spins in two adjacent trimers are ferromagnetically coupled along the a direction and antiferromagnetically coupled along the c direction (see Fig. S3 in Supplemental Material [22]).

IV. DISCUSSION AND CONCLUSION

As discussed previously, the obtained magnetic moment of $\text{Ba}_5\text{Ru}_3\text{O}_{12}$ based on Rietveld refinement to the neutron-diffraction data is about $3.79 \mu_B$ per Ru_3O_{12} trimer. For the RuO_6 octahedron, the d orbital splits into lower-energy t_{2g} and higher-energy e_g orbitals due to crystal-field effect in octahedral symmetry. Thus, considering discrete Ru atom, naively one would expect that Ru^{+4} (d^4) has four electrons in t_{2g} orbital which would yield $S = 1$ effective quantum number and that Ru^{+5} (d^3) yields $S = 3/2$ effective quantum number [see Fig. 7(a)]. This would give a total moment of $8 \mu_B$ (considering Landé g factor of 2) for three Ru atom, i.e., per Ru_3O_{12} trimer, which is much higher than the experimentally obtained moment of Ru_3O_{12} trimer. Therefore, other mechanisms need to be considered to account for the reduced magnetic moment in this system.

First, we consider molecular orbital of Ru_3O_{12} trimer with D_{3d} symmetry due to Ru-Ru metallic bonding, as proposed for some other trimer systems [4]. The $9R\text{-BaRuO}_3$ compound does not exhibit any magnetic ordering. The Ru-Ru distance is $\sim 2.53 \text{ \AA}$ which is shorter than Ru metal, yielding a hy-

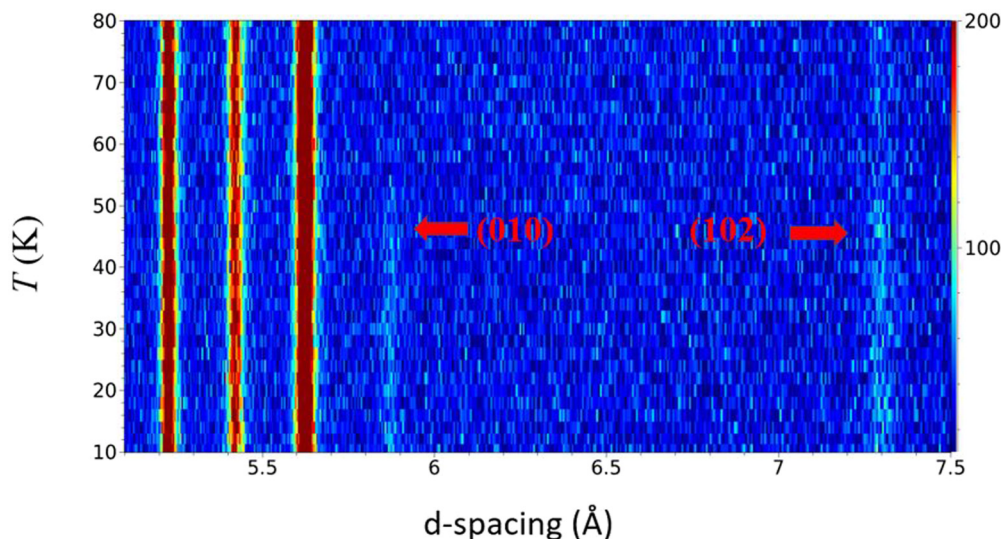


FIG. 6. Temperature- and d -dependent neutron-scattering intensity map. The red arrows point to the onset of magnetic transition.

bridization between d orbitals [23]. Because of this strong metal-metal bonding of Ru atoms within a trimer, the whole trimer may behave as a single molecular-orbital-like state instead of three discrete Ru orbitals, if the kinetic energy gain due to metallicity is larger than Coulomb interaction (Hund’s coupling). The total valence electron count of Ru_3O_{12} trimer is 12 ($\text{Ru}^{+4} \rightarrow d^4$). Considering the metal-metal bonding, the electronic configuration of a Ru_3O_{12} trimer with D_{3d} symmetry [24] is $(a_{1g})^2(e_g)^4(a_{2u})^2(e_u)^4$, which yields $S = 0$, and thus the compound behaves as a nonmagnet [18]. Similarly, metal-metal bonding with single molecular-like-orbital state has been predicted in another trimer compound $\text{Ba}_4\text{NbRu}_3\text{O}_{12}$, which consists of 13 electron in effective d orbital of Ru_3O_{12} trimer and thus yields an effective $S = 1/2$ in the trimer [4]. However, the same picture cannot be applied to $\text{Ba}_4\text{Ru}_3\text{O}_{10}$ ($\text{Ru}^{+4} \rightarrow d^4$) which exhibits magnetic ordering at 105 K with nonzero spin moment at Ru2 site of the trimer. And for $\text{Ba}_5\text{Ru}_3\text{O}_{12}$, it contains 10 valence electrons in total for each Ru_3O_{12} trimer. As a result, considering D_{3d} symmetry of Ru_3O_{12} trimer [24], that is, $(a_{1g})^2(e_g)^4(a_{2u})^2(e_u)^2$, one would anticipate $S = 1$ in its ground state [Fig. 7(b)]. The magnetic

moment obtained based on this model is smaller than the experimental value of this compound.

Second, we consider the effects of spin-orbit coupling. It is known that, in octahedral symmetry, the spin-orbit coupling (λ) may split the Ru orbital triplet ${}^3T_{1g}$ into three sublevels with energies $E = -2\lambda$ ($J = 0$), $E = -\lambda$ ($J = 1$), and $E = \lambda$ ($J = 2$). In this case, Ru^{4+} cations adopt $J = 0$ in its ground state and therefore the system would not order magnetically [18]. However, if the RuO_6 octahedra in trimers are not symmetrically connected in all direction, it may lift the degeneracy of the t_{2g} orbitals and thus lead to a ground state with nonzero magnetic moment. If we consider three discrete Ru orbitals instead of a single trimer-orbital picture, this model can account for the difference in the magnetic ground states of BaRuO_3 and $\text{Ba}_4\text{Ru}_3\text{O}_{10}$. For BaRuO_3 , the distortion of RuO_6 octahedron is small with the bond angle for $\text{O-Ru-O} \sim 180^\circ$, thus, the nonmagnetic $J = 0$ state can naturally apply to BaRuO_3 . In contrast, in $\text{Ba}_4\text{Ru}_3\text{O}_{10}$ the RuO_6 octahedron of Ru2 atom is slightly distorted with $\sim 171^\circ$ bond angle for the four in-plane O-Ru-O bonds and $\sim 180^\circ$ for the rest two O-Ru-O bonds with apical oxygen atoms. It is hypothetically argued

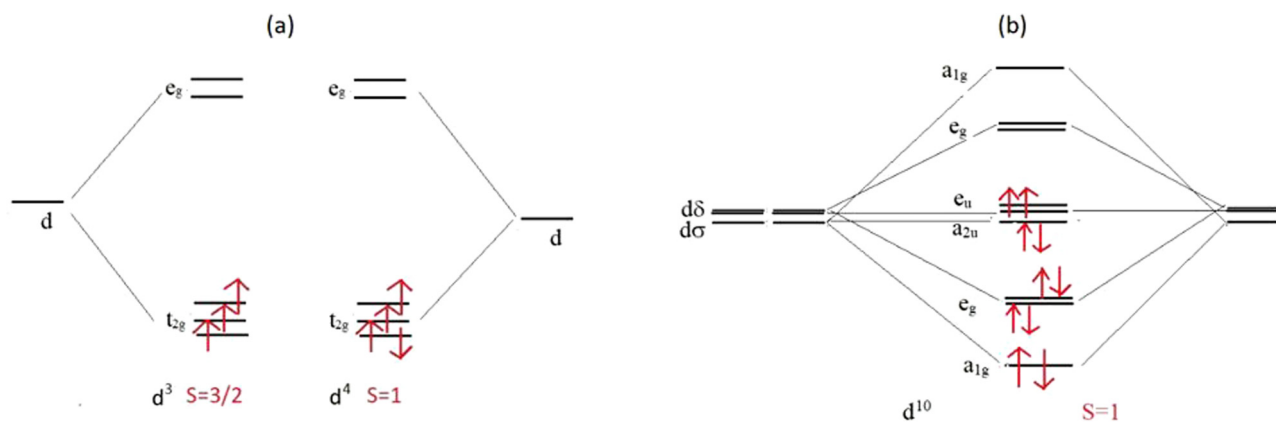


FIG. 7. (a) The electronic configuration of t_{2g} - e_g -model for d^3 and d^5 , and (b) electronic configuration of Ru trimer in D_{3d} symmetry due to metal-metal orbital hybridizations.

[18] that the perturbation of octahedral symmetry of Ru2 is large enough to lift the degeneracy of t_{2g} orbital but not for the Ru1. This results in nonzero moment of the ground state of two Ru atoms at edge of the trimer (Ru2) but zero moment of the center Ru atom of the trimer (Ru1). For $\text{Ba}_5\text{Ru}_3\text{O}_{12}$, there are three distinct Ru atoms, namely, Ru1, Ru2, and Ru3 and the average valence state is +4.67 (+5 for two Ru and +4 for one Ru). The Ru1-O distances are 1.98–2.0 Å, whereas, the Ru2-O and Ru3-O distances are 1.88–2.07 Å and 1.86–2.1 Å. The Ru-O-Ru angle for different Ru atoms are presented in Table I. Considering no spin-orbit coupling for Ru^{+5} (zero orbital degrees of freedom) and finite spin-orbit coupling for Ru^{+4} , the total moment of trimer ($S = 3/2$ for two Ru and $J = 0$ for one Ru) will be $6 \mu_B$, which is higher than the experimentally obtained value. Also, for $\text{Ba}_5\text{Ru}_3\text{O}_{12}$, as tabulated in in Table I, there is large deviation of the O-Ru-O bond angles from 180° , as observed in Ru2 atom for $\text{Ba}_4\text{Ru}_3\text{O}_{10}$, which also indicates that probably, this model (spin-orbit coupling) alone is not valid for our title compound.

Thus, the above two mechanisms that have been proposed for other trimers systems could not be applied individually to account for the experimentally obtained effective moment in $\text{Ba}_5\text{Ru}_3\text{O}_{12}$. It is likely that J_{nn} and J_{nnn} are comparable to each other and thus the competition between nearest- and next-nearest exchange interaction plays a crucial role for geometrical frustration, unlike BaRuO_3 and $\text{Ba}_4\text{Ru}_3\text{O}_{10}$ trimer systems. On the other hand, the different moment size of Ru on different crystallographic site indicates that orbital hybridization or/and spin-orbit coupling could be different for different Ru atoms. Our results suggest that the magnetism

in this compound is quite complex, on which the combined effects of different factors arising from geometrical frustration, spin-orbit coupling, and orbital hybridization determine the magnetic ground state. Further different spectroscopic and theoretical investigations are warranted to shed more light on this fascinating aspect.

In summary, our detailed investigation on $\text{Ba}_5\text{Ru}_3\text{O}_{12}$ trimer system reveals a long-range antiferromagnetic ordering below 60 K. A complex magnetism with canted spin structure is observed, distinct from other trimer systems such as BaRuO_3 , $\text{Ba}_4\text{Ru}_3\text{O}_{10}$, or $\text{Ba}_4\text{LnRu}_3\text{O}_{12}$. Such a complex behavior arises as a result of a combination of different level of hybridization (localization) on different Ru sites and strong spin frustration in this trimer system. The system exhibits insulating behavior throughout the temperature range measured. No metal-insulator-like transition is observed, unlike BaRuO_3 and $\text{Ba}_4\text{Ru}_3\text{O}_{10}$. This study demonstrates that the valence state and hybridization of Ru atom, together with the RuO_6 octahedral distortion, play an important role in electronic and magnetic correlations in ruthenates.

ACKNOWLEDGMENTS

Work at Michigan State University was supported by the US Department of Energy, Office of Science, Office of Basic Energy Sciences, Materials Sciences and Engineering Division under Award No. DE-SC0019259. A portion of this research used resources at Spallation Neutron Source, a DOE Office of Science User Facility operated by the Oak Ridge National Laboratory.

-
- [1] Y. Maeno, H. Hashimoto, K. Yoshida, S. Nishizaki, T. Fujita, J. G. Bednorz, and F. Lichtenberg, Superconductivity in a layered perovskite without copper, *Nature (London)* **372**, 532 (1994).
- [2] A. Banerjee, C. A. Bridges, J.-Q. Yan, A. A. Aczel, L. Li, M. B. Stone, G. E. Granroth, M. D. Lumsden, Y. Yiu, J. Knolle, S. Bhattacharjee, D. L. Kovrizhin, R. Moessner, D. A. Tennant, D. G. Mandrus, and S. E. Nagler, Proximate kitaev quantum spin liquid behaviour in a honeycomb magnet, *Nat. Mater.* **15**, 733 (2016).
- [3] J. Leshen, M. Kawai, I. Giannakis, Y. Kaneko, Y. Tokura, S. Mukherjee, W.-C. Lee, and P. Aynajian, Emergent charge order near the doping-induced mott-insulating quantum phase transition in $\text{Sr}_3\text{Ru}_2\text{O}_7$, *Commun. Phys.* **2**, 36 (2019).
- [4] L. T. Nguyen, T. Halloran, W. Xie, T. Kong, C. L. Broholm, and R. J. Cava, Geometrically frustrated trimer-based mott insulator, *Phys. Rev. Materials* **2**, 054414 (2018).
- [5] R. J. Cava, Schizophrenic electrons in ruthenium-based oxides, *Dalton Trans.* **19**, 2979 (2004).
- [6] P. Khalifah, R. Osborn, Q. Huang, H. W. Zandbergen, R. Jin, Y. Liu, D. Mandrus, and R. J. Cava, Orbital ordering transition in $\text{La}_4\text{Ru}_2\text{O}_{10}$, *Science* **297**, 2237 (2002).
- [7] T. Basu, V. Caignaert, S. Ghara, X. Ke, A. Pautrat, S. Krohns, A. Loidl, and B. Raveau, Enhancement of magnetodielectric coupling in 6H-perovskites $\text{Ba}_3R\text{Ru}_2\text{O}_9$ for Heavier Rare-Earth Cations ($R = \text{Ho}, \text{Tb}$), *Phys. Rev. Materials* **3**, 114401 (2019).
- [8] T. Basu, V. Caignaert, F. Damay, T. W. Heitmann, B. Raveau, and X. Ke, Cooperative $\text{Ru}(4d)$ - $\text{Ho}(4f)$ magnetic ordering and phase coexistence in the 6H perovskite multiferroic $\text{Ba}_3\text{HoRu}_2\text{O}_9$, *Phys. Rev. B* **102**, 020409(R) (2020).
- [9] M. Braden, O. Friedt, Y. Sidis, P. Bourges, M. Minakata, and Y. Maeno, Incommensurate Magnetic Ordering in $\text{Sr}_2\text{Ru}_{1-x}\text{Ti}_x\text{O}_4$, *Phys. Rev. Lett.* **88**, 197002 (2002).
- [10] K. Yoshida, F. Nakamura, T. Goko, T. Fujita, Y. Maeno, Y. Mori, and S. Nishizaki, Electronic crossover in the highly anisotropic normal state of Sr_2RuO_4 from pressure effects on electrical resistivity, *Phys. Rev. B* **58**, 15062 (1998).
- [11] M. Zhu, J. Peng, W. Tian, T. Hong, Z. Q. Mao, and X. Ke, Tuning the competing phases of bilayer ruthenate $\text{Ca}_3\text{Ru}_2\text{O}_7$ via dilute Mn impurities and magnetic field, *Phys. Rev. B* **95**, 144426 (2017).
- [12] L. Klein, J. S. Dodge, C. H. Ahn, J. W. Reiner, L. Mievilte, T. H. Geballe, M. R. Beasley, and A. Kapitulnik, Transport and magnetization in the badly metallic itinerant ferromagnet SrRuO_3 , *J. Phys.: Condens. Matter* **8**, 10111 (1996).
- [13] L. Klein, L. Antognazza, T. H. Geballe, M. R. Beasley, and A. Kapitulnik, Possible non-fermi-liquid behavior of CaRuO_3 , *Phys. Rev. B* **60**, 1448 (1999).
- [14] J. G. Zhao, L. X. Yang, Y. Yu, F. Y. Li, R. C. Yu, Z. Fang, L. C. Chen, and C. Q. Jin, Structural and physical properties of the 6H BaRuO_3 polymorph synthesized under high pressure, *J. Solid State Chem.* **180**, 2816 (2007).

- [15] J. T. Rijssenbeek, R. Jin, Yu. Zadorozhny, Y. Liu, B. Batlogg, and R. J. Cava, Electrical and magnetic properties of the two crystallographic forms of BaRuO_3 , *Phys. Rev. B* **59**, 4561 (1999).
- [16] C. Dussarrat, F. Grasset, R. Bontchev, and J. Darriet, Crystal structures and magnetic properties of $\text{Ba}_4\text{Ru}_3\text{O}_{10}$ and $\text{Ba}_5\text{Ru}_3\text{O}_{12}$, *J. Alloys Compd.* **233**, 15 (1996).
- [17] T. Igarashi, Y. Nogami, Y. Klein, G. Rousse, R. Okazaki, H. Taniguchi, Y. Yasui, and I. Terasaki, X-ray crystal structure analysis and Ru valence of $\text{Ba}_4\text{Ru}_3\text{O}_{10}$ single crystals, *J. Phys. Soc. Jpn.* **82**, 104603 (2013).
- [18] Y. Klein, G. Rousse, F. Damay, F. Porcher, G. André, and I. Terasaki, Antiferromagnetic order and consequences on the transport properties of $\text{Ba}_4\text{Ru}_3\text{O}_{10}$, *Phys. Rev. B* **84**, 054439 (2011).
- [19] S. V. Streltsov and D. I. Khomskii, Unconventional magnetism as a consequence of the charge disproportionation and the molecular orbital formation in $\text{Ba}_4\text{Ru}_3\text{O}_{10}$, *Phys. Rev. B* **86**, 064429 (2012).
- [20] J. Rodríguez-Carvajal, Recent advances in magnetic structure determination by neutron powder diffraction, *Physica B: Condens. Matter* **192**, 55 (1993).
- [21] A. S. Wills, A new protocol for the determination of magnetic structures using simulated annealing and representational analysis (SARAh), *Physica B: Condens. Matter* **276-278**, 680 (2000).
- [22] See Supplemental Material at <http://link.aps.org/supplemental/10.1103/PhysRevMaterials.4.114401> for neutron diffraction analysis and magnetic structure of $\text{Ba}_4\text{Ru}_3\text{O}_{10}$ compound.
- [23] Y. A. Ying, Y. Liu, T. He, and R. J. Cava, Magnetotransport properties of BaRuO_3 : Observation of two scattering rates, *Phys. Rev. B* **84**, 233104 (2011).
- [24] B. E. Bursten, F. A. Cotton, and A. Fang, Ground-state electronic structures and other electronic properties of the octahedral and oligooctahedral ruthenium complexes hexachlororuthenium(III), nonachlorodiruthenium(III) and dodecachlorotriruthenium(II, 2III), *Inorg. Chem.* **22**, 2127 (1983).